Rotating-Top Approximation in Reduced-Dimensionality Quantum Calculations of Rate Constants: Application to Complex-Forming Nucleophilic Substitution†

Carsten Hennig and Stefan Schmatz*

Institut für Physikalische Chemie, Universität Göttingen, Tammannstr. 6, D-37077 Göttingen, Germany

Received: June 28, 2005; In Final Form: August 19, 2005

Within the framework of reduced-dimensionality quantum scattering theory, we employ Bowman's adiabatic rotation approximation to describe reactive systems that have symmetric-top geometries during the entire collision process. The results are compared with the approach of shifting the total energy by a characteristic rotational energy. Initial state-selected and total thermal rate constants have been computed for the complex-forming gas-phase reaction $Cl^- + CH_3Cl' \rightarrow ClCH_3 + Cl'^-$. At room temperature, we find a significant contribution from energetically high vibrational modes. The dependence of the cross-sections on the different angular momenta is analyzed in detail, and high total angular momenta are found to be of considerable importance. The influence of adiabatic azimuthal rotation on the rate constants turns out to be small compared to other effects. In addition, we use a new model to account for the asymmetric modes not explicitly contained in the scattering calculations. The difference to the only available experimental value confirms our conclusion that the Cl−C−Cl′ bending modes are of major importance for this reaction.

I. Introduction

For reactions involving polyatomic molecules, the calculation of converged quantum-mechanical reaction probabilities and cross-sections is a formidable task. Usually, only a selection of the internal degrees of freedom of the system can be considered. By employing simple energy-shifting procedures,[1−6] the calculation of thermal rate constants is possible by including the degrees of freedom which are not explicitly taken into account quantum-mechanically. Moreover, the overall rotational motion is usually considered by shifting the reaction probability for total angular momentum $\boldsymbol{J} = 0$ by the rotational energies of the transition state complex. This procedure could be applied quite successfully for reactions proceeding over a simple barrier, while for complex-forming systems, where the reaction probability is governed by sharp resonance features, *J*-shifting is highly questionable.

With a more sophisticated approach in reduced-dimensionality quantum scattering calculations, approximate probabilities for $\boldsymbol{J} \neq 0$ can be obtained by applying the rotating-line approximation (RLA)[7] that has been widely used in the past. This method is suitable for collinear reactions with a linear transition state complex and thus a single rotational constant. However, most reactions involving polyatomic molecules do not proceed via transition states with collinear alignment of all nuclei. For example, for symmetric tops, the projection of $\boldsymbol{J}$ on the molecular axis of symmetry has to be taken into account. In this work, we modify the adiabatic rotation approximation (ARA) advocated by Bowman[8−10] to a simplified version, the rotating (symmetric) top approximation (RTA), which can be applied in the calculation of rate constants from reduced-dimensionality quantum scattering data for true symmetric-top geometries during the entire collision process (not only at the transition state).

Complex-forming bimolecular reactions are particularly challenging for studying the applicability of such dimensionality-reduced models, because they have turned out to be very sensitive with respect to shifting procedures. Prototypes for this class of reactions are gas-phase nucleophilic bimolecular substitution (S_N2) reactions.[11−14] In particular, the halogen exchange Walden inversion reactions

$$X^- + CH_3Y \rightarrow XCH_3 + Y^- \qquad (1)$$

where X and Y are halogen atoms have been investigated in detail both from the experimental and the theoretical side (see refs 15−47 and references cited in refs 11−14). Because of the long-range electrostatic attraction between the collision partners, the depths of the entrance and exit channel wells on the potential energy surface (PES) are considerable (ca. 0.5 eV).[11−16,23] Detailed quantum dynamical studies[38,39,41,43,44] have given evidence that very sharp resonance structures dominate the dynamics of gas-phase S_N2 systems. The widths of neighboring resonances cover a range of more than 4 orders of magnitude. These resonances are of Feshbach type and, in exothermic systems, e.g., $Cl^- + CH_3Br$, are also of shape type. They are connected with the long-lived intermediates $X^-\cdots CH_3Y$ and $XCH_3\cdots Y^-$ that are formed in the entrance and exit channels of the reaction.

Experiments on the detailed, state-selected dynamics of gas-phase S_N2 reactions are scarce. Ervin et al.[24] studied the promotion of the symmetric reaction

$$Cl^- + CH_3Cl' \rightarrow ClCH_3 + Cl'^- \qquad (2)$$

by kinetic energy, employing guided ion beam tandem mass spectrometry. Making use of the tandem flowing afterglow-SIFT technique, Bierbaum and co-workers[17] could determine the thermal rate coefficient for this reaction at 300 K to be $k = (3.5 \pm 1.8) \times 10^{-14}$ cm^3 s^{-1}.

Computationally, Hase and co-workers[19−22,26,27,29,37] pointed out in their work on the classical dynamics of gas-phase S_N2 reactions that the coupling between the inter- and intramolecular

† Part of the special issue "William Hase Festschrift".

* Corresponding author. Electronic mail: sschmat@gwdg.de.

10.1021/jp053521n CCC: $33.50 © 2006 American Chemical Society
Published on Web 10/20/2005

modes of the collision complexes is only weak, causing inefficient energy transfer.

Total quantum mechanical cross-sections $\sigma(E)$ can be obtained as weighted sums over reactions probabilities $P^J(E)$ for all total angular momenta $\boldsymbol{J}$ at given energy E. In a recent paper, Hennig and Schmatz[45] reported four-mode quantum scattering calculations on initial state-selected total cross-sections and the rate constant for the above S_N2 reaction (2). After reducing the dimensionality, the system was studied under the restriction that C_{3v} symmetry is maintained throughout the course of reaction. It turned out that rotational effects must play a crucial role in the dynamics.

It is now important to see how the results change when the rotating-top approximation is employed instead of the rotating-line approximation. Furthermore, the rate constant calculation can be extended by a more accurate inclusion of the high-frequency modes not yet explicitly incorporated in the model. Moreover, a thorough analysis of the convergence of rate constants with respect to total angular momentum quantum number J in the J-shifting and RTA approximations is very useful to understand the limitations of the models. Finally, a detailed analysis of the contributions of the various initial vibrational states to the rate constants at different temperatures should shed more light on the underlying dynamics.

The paper is organized as follows: In section II, we introduce the RTA and briefly describe the Hamiltonian and the reactive scattering formalism as well as the reduced-dimensionality theory to recover the full-dimensional thermal rate constant; furthermore, numerical details of our computations are given. Section III presents the results and their discussion. Finally, section IV contains our conclusions. Throughout this work, energies are quoted in wavenumber units.

II. Theory

A. Rotating-Top Approximation. Within the rotating-line approximation (RLA)[7] for collinear reactions formulated in hyperspherical coodinates, a centrifugal term is added to the scattering Hamiltonian for $J = 0$, $\hat{H}^{J=0}$,

$$\hat{H}^J = \hat{H}^{J=0} + \frac{\hbar^2 J(J+1)}{2\mu\rho^2} \tag{3}$$

so that reaction cross-sections can be calculated. Here, J is the total angular momentum quantum number. For true symmetric-top systems, this model can be extended to a rotating-top approximation, where we add the term

$$\hat{H}^{JK} = \hat{H}^{J=0} + B_{\mathrm{eff}}(\rho)[J(J+1) - K^2] + A(\rho)K^2 \tag{4}$$

with $-J \le K \le J$. Here, A and B_{eff} denote the two rotational constants of a prolate symmetric top,

$$B_{\mathrm{eff}}(\rho) = \frac{\hbar^2}{2\mu\rho^2} \tag{5}$$

and

$$A(\rho) = \frac{\hbar^2}{2\sum_i m_i q_i^2(\rho)}, \tag{6}$$

where the q_i values are the perpendicular distances of the nuclei of mass m_i from the molecular axis of symmetry.

It has to be emphasized that this Hamiltonian can be derived equivalently from the more general adiabatic rotation approximation (ARA) of Bowman.[8−10] In this method, the rotational energy of the collision system is calculated at a given configuration, and the resulting (adiabatic) rotational energy is then added to the potential energy, forming an effective potential. Bowman's method in turn relates to the optimum helicity conserving approximation of McCurdy and Miller.[48] For the complex-forming system $O(^1D) + HCl$, the ARA has been used to determine the rotational barriers.[49] Moreover, the ARA has been successfully applied to triatomic reactive scattering by other groups, both within the time-independent (for $Cl + H_2$ and $F + H_2$)[50] and time-dependent (for $N^+ + H_2$)[51] approaches. Note that in ref 50 a hyperspherical coordinate coordinate system was also used. In the present approach, the diagonalization of the inertia tensor is not necessary because in the given reduced-dimensionality model, the system is always a true symmetric top. In this sense, our approach is also closely linked to the centrifugal sudden approximation (CSA).[52,53]

B. Hamiltonian. Within the dimensionality-reduced 4D model described in detail in refs 43 and 44, we employ a C_{3v} symmetric approach and hence study the reaction

$$X^- + CH_3Y(v_1, v_2, v_3) \rightarrow XCH_3(v_1', v_2', v_3') + Y^-. \tag{7}$$

In eq 7, v_i and v_i' ($i = 1, 2, 3$) denote the quantum numbers of the symmetric C−H stretching (v_1, v_1'), the umbrella bending (v_2, v_2'), and the C−Hal stretching (v_3, v_3') vibrational modes in reactant and product methyl halides, respectively.

We describe the totally symmetric dynamics of the methyl group by orthogonal coordinates q and z (see ref 43 for details); employing Jacobi coordinates for the C−Hal stretching degrees of freedom completely decouples the kinetic energy. After mass-scaling and transformation to hyperspherical coordinates ρ and δ,[54−59] the completely orthogonal Hamiltonian

$$\hat{H} = -\frac{\hbar^2}{2\mu_1}\left(\frac{\partial^2}{\partial\rho^2} + \frac{1}{4\rho^2}\right) - \frac{\hbar^2}{2\mu_1\rho^2}\frac{\partial^2}{\partial\delta^2} - \frac{\hbar^2}{2\mu_2}\frac{\partial^2}{\partial z^2} - \frac{\hbar^2}{2\mu_3}\frac{\partial^2}{\partial q^2} + V(\rho, \delta, z, q) \tag{8}$$

is obtained. The latter four terms including the potential define the three-dimensional (3D) so-called surface Hamiltonian $\hat{H}_{\mathrm{surf}}$ that only parametrically depends on the hyperradius ρ. The reduced masses are given by $\mu_1 = [m_X m_{CH_3} m_Y/(m_X + m_{CH_3Y})]^{1/2}$, $\mu_2 = 3m_H m_C/(3m_H + m_C)$ and $\mu_3 = 3m_H$, where m_C and m_H denote the masses of the isotopes ^{12}C and ^1H. In the present case, $m_X = m_Y = m^{35}_{Cl}$. For the S_N2 reaction, we obtain the A rotational constant to be

$$A(\rho) = \frac{\hbar^2}{6m_H q^2(\rho)} \tag{9}$$

where $q = r_{CH} \sin\theta$. Here, θ is the H−C−Y angle and r_{CH} is the C−H distance of all three C−H bonds.

C. Reactive Scattering Formalism. For given angular momentum quantum numbers J and K and total energy E, the Schrödinger equation $\hat{H}^{JK}\Psi^{JK}(\rho, \delta, z, q) = E\Psi^{JK}(\rho, \delta, z, q)$ is solved in two steps to obtain the partial waves Ψ^{JK}. In every sector, we expand the partial wave $\Psi^{JK}_{n'}$ for initial state n' in close-coupling form[44]

$$\Psi^{JK}_{n'}(\rho; \rho_i; \delta, z, q) = \rho^{-1/2}\sum_{n=1}^{N} g^{JK}_{n'n}(\rho; \rho_i)\Phi_n(\delta, z, q; \rho_i) \tag{10}$$

with N denoting the total number of channels. As described in detail in ref 44, $\hat{H}_{surf}$ is diagonalized in a suitable potential optimized (PO) sinc-DVR basis.[60,61] The R-matrix method[62] is employed for the propagation of the radial functions $g^{JK}_{n'n}$. Overlap matrices between eigenfunctions of adjacent sectors are computed only once and are then used in the subsequent R-matrix propagations for all values of E, J and K. Boundary conditions in the asymptotic region of the potential are applied according to ref 45. The R-matrix propagation is repeated for all values of J and K possible for total energy E.

The K-dependent reactive scattering cross-sections are then given by

$$\sigma^K_{i,f}(E) = \frac{\pi}{k_i^2}\sum_{J=K}^{\infty}(2J+1)P^{JK}_{i,f}(E) \tag{11}$$

with $P^{JK}_{i,f}(E) = |S^{JK}_{i,f}(E)|^2$. Note that the summation starts at K, not zero. The collective quantum numbers $i = (v_1, v_2, v_3)$ and $f = (v_1', v_2', v_3')$ denote the initial and final states, respectively, of CH_3Cl. Here, k_m^2 is given by

$$k_m^{\,2} = \frac{2\mu_1}{\hbar^2}(E - \epsilon_m) \tag{12}$$

with ϵ_m the asymptotic energy of channel m, and $E - \epsilon = E_{trans}$.

D. Reduced-Dimensionality Calculations of the Thermal Rate Constant. By employing the full-dimensional cumulative reaction probability

$$P^{full}_{cum}(E) = \sum_{i,f}\sum_{J=0}^{\infty}(2J+1)P^J_{i,f}(E) \tag{13}$$

the thermal rate constant can be calculated exactly by

$$k(T) = \frac{1}{hQ_r}\int_0^{\infty} e^{-E/(k_BT)}\, P^{full}_{cum}(E)\, dE \tag{14}$$

where h and k_B are Planck's and Boltzmann's constants, respectively, while $Q_r = Q_{int}Q_{trans}$ is the partition function per unit volume for the reactants.

The dimensionally reduced (RD) theory for the calculation of thermal rate constants is based on energy-shifting procedures for the modes that are not treated explicitly.[1−6] Our C_{3v} model for halogen-exchange S_N2 reactions considers the four modes of a_1 symmetry explicitly, while the influence of the other modes is taken into account by energy shifting

$$P^{full}(E) \approx \sum_k P^{4D}(E - E^{\dagger}_k) \tag{15}$$

where the index k collectively denotes the quantum numbers of the four doubly degenerate (e symmetry) vibrational modes of the transition state complex that are not explicitly included in the 4D RD model. The vibrational energy levels of the transition states, $E^{\dagger}_k$, are measured relative to zero-point energy and are calculated for an ensemble of eight harmonic oscillators.

In the J-shifting/K-shifting approximation,[10] only the reaction probability $P^{J=0}(E) = \sum_{i,f}P^{J=0}_{i,f}$, summed over all initial and final states, is determined for $K = 0$ and shifted by the rotational energies of the transition state according to

$$P^J(E) = \sum_{K=-J}^{J} P^{J=0}(E - E^{JK}). \tag{16}$$

Here, E^{JK} is the symmetric-top energy $B^{\dagger}J(J+1) + (A^{\dagger}-B^{\dagger})K^2$ with $A^{\dagger}$ and $B^{\dagger}$ being the rotational constants of the prolate symmetric-top saddle point species. Employing this approximation, one obtains

$$k(T) = \frac{Q^{\dagger}_{red}Q^{\dagger}_{rot}\, e^{-\Delta_0/(k_BT)}}{hQ_{int}Q_{trans}}\int_0^{\infty} e^{-E/(k_BT)}\sum_{i,f}P^{J=0}_{i,f}(E)\, dE \tag{17}$$

where $Q^{\dagger}_{red}$ denotes the partition function of the four degenerate internal modes in the transition state, while $Q^{\dagger}_{rot}$ is the corresponding rotational partition function. Q_{trans} is the 3D translational partition function, and Q_{int} denotes the partition function for all internal degrees of freedom of the reactants, i.e., for all vibrational modes and rotations of CH_3Cl.

The quantity Δ_0 denotes the difference of the zero-point energies between the saddle point structure and the reactant with respect to the four e modes. Thus, Δ_0 recovers the vibrationally adiabatic ground-state barrier height of the full-dimensional PES. In the RLA, reaction probabilities are calculated for each J individually by using the Hamiltonian $\hat{H}^J$. Usually, K is set to zero in this calculation, and probabilities for $K > 0$ are obtained by an analogous energy-shifting procedure (K-shifting)

$$P^{JK}(E) \approx P^J(E - E^K) \tag{18}$$

for $K = -J, ..., J$. E^K is the azimuthal part of E^{JK}, $E^K = (A^{\dagger} - B^{\dagger})K^2$. This results in the K summation still being included in the energy integration when computing the rate constant, cf. eq 13 in ref 45.

In the RTA, we instead calculate reaction probabilities for each energetically allowed combination of J and K by employing $\hat{H}^{JK}$, proceeding by

$$P_{i,f}(E) = \sum_{J=0}^{\infty}(2J+1)\sum_{K=-J}^{J}P^{JK}_{i,f}(E) = \sum_{J=0}^{\infty}(2J+1)\sum_{K=0}^{J}(2\text{-}\delta_{K0})P^{JK}_{i,f}(E) \tag{19}$$

and thus obtaining for the rate constant

$$k(T) = \frac{Q^{\dagger}_{red}\, e^{-\Delta_0/(k_BT)}}{hQ_{int}Q_{trans}}\int_0^{\infty} e^{-E/(k_BT)}\sum_{J=0}^{\infty}(2J+1)\times \sum_{K=0}^{J}(2-\delta_{K0})\sum_{i,f}P^{JK}_{i,f}(E)\, dE. \tag{20}$$

Each of these models also allows one to compute state-selective rate constants by specifying an initial state i and summing only over the final states f.

It should by noted that, in addition to eq 18, it is also possible to compute reaction probabilities for $K > 0$ from those for $K = 0$ by shifting to the corresponding translational energy

$$P^K(E) \approx P^{K=0}(E - E^K_{trans}) \tag{21}$$

where $P^{K=0}$ is obtained by summing over all $P^{J,K=0}$, and $E^K_{trans} = B(\rho_{end})K + A(\rho_{end})K^2$ is the energy difference between $K = 0$ and an arbitrary K for $J = K$ at the final hyperspherical radius ρ_{end} (the first term in this expression becomes vanishingly small for $\rho \rightarrow \infty$). The first approach as described in eq 18 refers to the transition state and is thus appropriate for the numerator in the expression used to compute rate constants, whereas the

latter procedure aims at the asymptotic configuration. It is therefore used in the comparison of cross-sections for different K values at the same translational energy. Both will be called K-shifting with the distinction given by the context.

E. Asymmetric Mapping. All of the above models essentially map the degrees of freedom not explicitly considered onto the vibrational ground state; see eq 15. For those degrees of freedom which are expected to actively take part in the reaction, this is quite a poor approximation and used mainly because of the absence of a suitable alternative. However, for the two doubly degenerate vibrations of the methyl group, a reference to the corresponding explicitly treated totally symmetric modes is feasible. While a mapping to the ground state will underestimate the reactivity, using the symmetric modes yields an upper bound for the influence of these degrees of freedom.

In extension of eq 15, we need to specify state-selective probabilities $P_i(E)$ for an initial state i, summed over all final states, by the ansatz

$$P_i(E) \approx P_{i'}^{4D}(E - \Delta_0 - E^{\dagger} - \alpha) \tag{22}$$

where i' is the explicitly treated state corresponding to i, i.e., all quanta that do not correspond to an explicitly treated mode are removed and each quantum in one of the two doubly degenerate asymmetric internal modes of the CH_3 group is replaced by one in the corresponding totally symmetric mode. As in eq 15, $E^{\dagger}$ denotes the vibrational energy levels of the transition states of all modes mapped onto the ground state, while α incorporates the energy difference between the asymmetric and symmetric modes at the transition state. Both energetic quantities are evaluated in the harmonic approximation. As $\alpha < 0$, this will effectively reduce the probabilities in the asymmetric modes compared to the symmetric ones, which is consistent with their expected behavior.

As a consequence for every initial state $i = (\upsilon_1, \upsilon_2, \upsilon_3)$, $k = 0, ..., \upsilon_1$ of the υ_1 quanta in the symmetric C−H stretching vibration can be created by originally storing them in its doubly degenerate counterpart mode. For a given k, this will result in a factor $(k + 1)e^{-k\alpha_1/(k_BT)}$ where $\alpha_1 = -192$ cm^{-1} is the difference between the harmonic wavenumbers of the symmetric and asymmetric C−H stretching modes at the transition state; the exponential term stems from the energy shift by α when integrating over energy in eq 22, while the factor $k + 1$ accounts for the degeneracy. The same consideration holds for the υ_2 quanta in the umbrella mode, which can be can be created by originally storing $l = 0, ..., \upsilon_2$ quanta in the doubly degenerate asymmetric counterpart; here, the energy shift amounts to $l\alpha_2$ with $\alpha_2 = -400$ cm^{-1} being the difference of the symmetric umbrella mode to the asymmetric H−C−H bending vibration at the transition state.

By summing over k and l, we conclude that the probability $P_i(E)$ for each initial state $i = (\upsilon_1, \upsilon_2, \upsilon_3)$ will be weighted by a factor

$$\sum_{k=0}^{\upsilon_1}(k+1)\, e^{-k\alpha_1/(k_BT)} \sum_{l=0}^{\upsilon_2}(l+1)\, e^{-l\alpha_2/(k_BT)}. \tag{23}$$

Using

$$g_{n+1}(q) = \sum_{k=0}^{n}(k+1)q^k = \frac{1 - q^{n+2} - (n+2)q^{n+1}(1-q)}{(1-q)^2} \tag{24}$$

for $n = 0, 1, 2, ...$, we finally obtain for the rate constant

$$k(T) = \frac{Q_{(-e)}^{\dagger}\, e^{-\Delta_0/(k_BT)}}{hQ_{int}Q_{trans}} \times \int_0^{\infty} dE\, e^{-E/(k_BT)} \sum_{i=(v_1,v_2,v_3)} P_i(E) g_{\upsilon_1+1}(e^{-\alpha_1/(k_BT)}) g_{\upsilon_2+1}(e^{-\alpha_2/(k_BT)}). \tag{25}$$

Dependence on J and K including the summation has been suppressed in eq 25 for clarity and must be included in accordance with each of the models presented in section 2.4. $Q_{(-e)}^{\dagger}$ is the partition function for the degrees of freedom at the transition state appropriate for the selected model excluding the two doubly degenerate asymmetric internal modes of the methyl group. In our RTA model, $Q_{(-e)}^{\dagger}$ contains the partition function of the two remaining doubly degenerate modes at the transition state, i.e., the Cl−C−Cl bending and the CH_3 rocking modes.

F. Numerical Details. The 4D PES from ref 43 with classical barrier height of 984 cm^{-1} is employed with the asymptotic energy set to zero. Unless stated otherwise, all energies in the dynamics calculations are counted from the asymptotic vibrational ground state of CH_3Cl.

All parameters used in the quantum scattering calculations reported in this work are collected in Table 1 of ref 45. In the propagation of the partial waves, the number of channels actually taken into account (all open channels and ten additional closed channels) depended on the sector ρ_i. In the potential wells, a lower number of channels was chosen for higher energies, because the energetically highest computed state in this region lies at ca. 3250 cm^{-1}. With this restriction, all channels below an energy of 3220 cm^{-1} were additionally included in each sector in computations with an energy below that limit. The S-matrices and thus reaction probabilities have been computed for total energies E_{tot} up to 6000 cm^{-1} above the asymptotic vibrational ground state of CH_3Cl.

The energetic resolution ΔE was at least 10 cm^{-1} with a much finer grid in the low-energy regime: $\Delta E = 10^{-1}$ cm^{-1} for $E_{tot} \le 250$ cm^{-1} and $\Delta E = 1$ cm^{-1} for 250 cm^{-1} $\le E_{tot} \le$ 1600 cm^{-1}. Convergence especially in the low-temperature regime has been checked by comparison with rate constants obtained from a refinement for $K = 0$: $\Delta E = 10^{-2}$ cm^{-1} for $E_{tot} \le 100$ cm^{-1} and $\Delta E = 1$ cm^{-1} up to $E_{tot} \le 1720$ cm^{-1}. This refinement results in an increase of the rate constant by a factor of at most 2.5 for very low temperatures and hardly any change for temperatures above 100 K.

Rotational partition functions were calculated in the rigid rotor model by explicit summation. For a given ρ, $V(\delta, z, q; \rho_i)$ was minimized to obtain the optimal $q(\rho)$ value for $A(\rho)$.

For the highest energies considered, total angular momenta up to ca. $J = 1200$ and azimuthal angular momenta $K = 33$ have been computed; in the energetic region up to $E_{tot} = 1600$ cm^{-1} relevant at room temperature, partial waves up to ca. $J = 500$ and $K = 16$ still have to be considered. The computational effort thus rises by a factor of 10−30 in the RTA model compared to K-shifting in the RLA model; the RLA model itself requires about 200−1000 more partial waves than the simple J-shifting model. The total increase in CPU and storage requirements of the RTA model compared to J-shifting is thus about 4 orders of magnitude. This is the reason for the much coarser grid compared to our previous calculations: For $J = 0$,[44] a computationally demanding energy grid of $\Delta E = 10^{-3}$ cm^{-1} down to $\Delta E = 10^{-12}$ cm^{-1} was necessary to resolve all the narrow resonances. From the above considerations, it is not

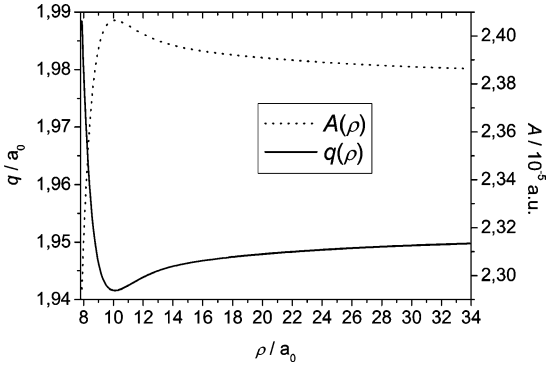

Figure 1. Changes of the orthogonal coordinate q and the symmetric-top rotational constant A during the reaction (as a function of the hyperradius ρ).

possible to use the same energy resolution in the RLA/RTA model, resulting in a not fully converged resonance structure of the individual partial waves. However, summation leads to an averaging and broadening of the resonances. As demonstrated by the analysis of the contributions of individual angular momenta (see below, Figure 9), the rate constants, which are additionally energy-averaged quantities, are correct in the order of magnitude for low temperatures; for room temperature and above, the obtained values are converged with respect to the energetic resolution.

III. Results and Discussion

A. *K*-Dependent Reaction Cross-Sections. Figure 1 graphically displays the variations of the two most important structural parameters of the C_{3v} symmetric methyl group, the rotational constant $A(\rho)$ and $q(\rho)$, the distance between one hydrogen nucleus, and the molecular axis of symmetry. For each value of the hyperradius ρ, the geometries were optimized with respect to energy. The formation of the complex results in a slight shortening of the C−H bond distance and consequently of q, whereas at even shorter distances, the H-atoms are pushed away by the energetically unfavorably close Cl-atoms. The resulting ρ-dependent variation of A influences the final reaction cross-sections via the changes of the available kinetic energy during the propagation.

The cumulative reaction cross-sections summed over all final states and all possible values of the azimuthal quantum number K, $\sum_f \sum_K \sigma_{i,f}^K(E)$, are shown in Figure 2. The small cross-section for the reaction out of the vibrational ground state and those for initial excitation of the C−Cl and C−H stretching modes [(0, 0, 1) and (1, 0, 0)], as well the combination mode (1, 0, 1), are displayed as a function of translational energy on a logarithmic scale in Figure 2a. Figure 2b shows reaction cross-section sums as a function of total energy when the vibration of the broken C−Cl bond is excited by one to eight quanta, while Figure 2c displays—for the same range of total energy—the cross-section sums for initial excitation of the umbrella bending mode with one to four quanta. Finally, some cross-section sums for initially excited combination modes of C−Cl stretch and umbrella bend are shown. The data can be compared to the $K = 0$ cross-sections from ref 45. Some of the differences are simply caused by the different setting: In contrast to ref 45, the data in Figure 2 has been averaged over intervals of 80 cm^{-1}, resulting in less structure and acuteness. As we show cumulative cross-sections summed over all K, the scale of the ordinates changes by several orders of magnitude. However, some of the features in Figure 2 could not be so easily predicted from our previous calculations: The envelope of the maxima becomes smoother; in Figure 2b, the increase of the maxima has become much more monotonic (dips at $\upsilon_3 = 3$, 5,

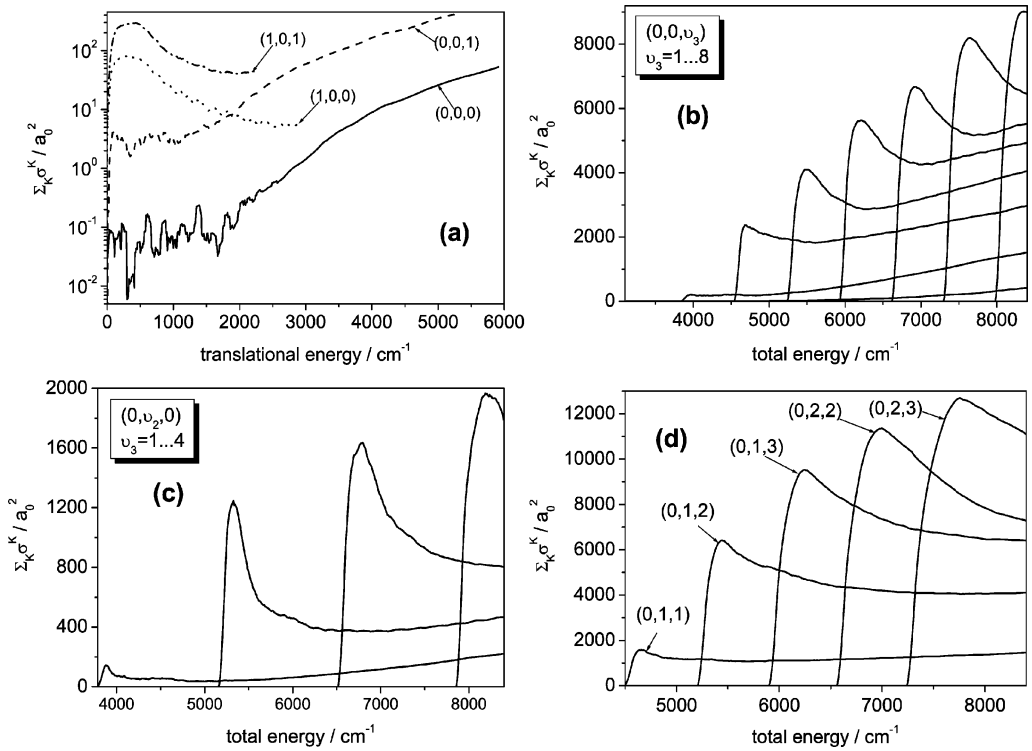

Figure 2. Initial state-selected total reaction cross-sections for the reaction $Cl^- + CH_3Cl'$ (υ_1, υ_2, υ_3) → $ClCH_3 + Cl'^-$, summed over all accessible product channels and all values of the quantum number K. The data are averaged over intervals of 80 cm^{-1}. (a) As a function of translational energy, (b−d) as a function of total energy, counted from the classical asymptotic limit. (a) Reaction out of the reactant vibrational ground state and excited states (0, 0, 1), (0, 1, 0), (1, 0, 0) and (1, 0, 1). (b) Excitation of the C−Cl stretching mode ν_3 with up to eight quanta. (c) Excitation of the umbrella bending mode ν_2 with with up to four quanta. (d) Excitation of selected combination modes.

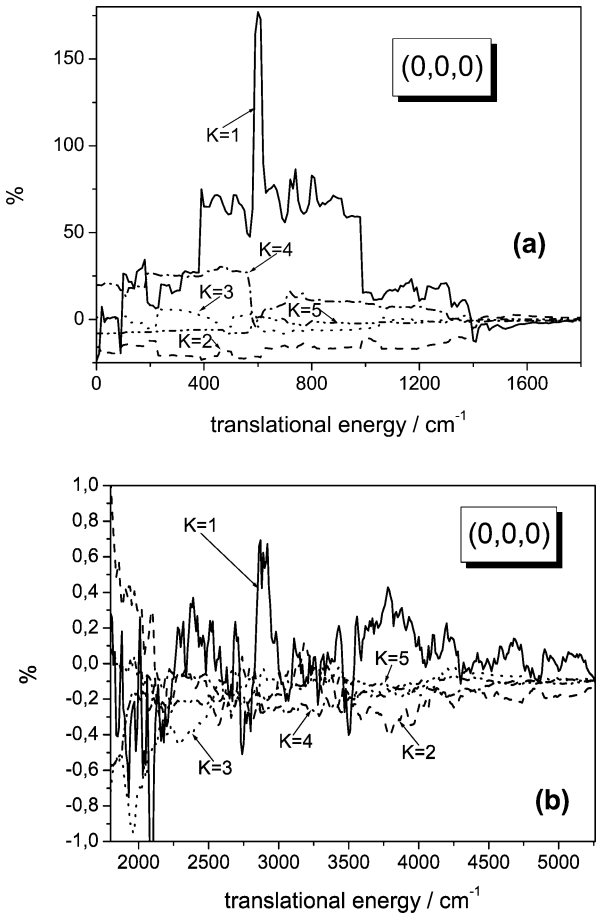

Figure 3. Relative deviation $d_i^k(E)$ of the state-selected cross-section for initial state (0, 0, 0) for azimuthal quantum number K from the one for $K - 1$, weighted by the difference of the squares of the azimuthal quantum numbers (see the text). Each cross-section is evaluated at the same translational energy E. The data are averaged over 600 cm^{-1}.

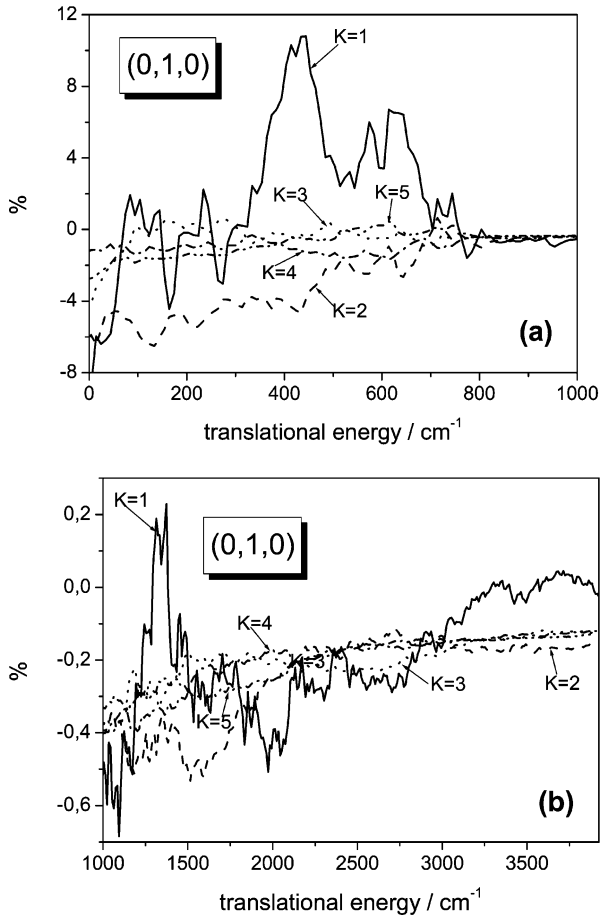

Figure 4. Same as Figure 3 for initial vibrational state (0, 1, 0).

and 7 are missing). Also in Figure 2d, some curves change order with respect to their maxima [e. g., (0, 2, 2) and (0, 2, 3)]. For large values of the total energy, nearly all curves show a deviation from the $1/k^2_i$ behavior, which is explained by the presence of several of these prefactors due to the summation over different initial states (different K). Finally, in Figure 2a, the C−H-stretching mode does not reach the spectator mode regime valid for higher translational energies in contrast to ref 45, where such a spectator-mode behavior can be observed within the displayed energy range. We attribute this to the contribution of cross-sections with higher K and thus lower translational energy.

To assess the influence of different values of K on the cross-sections, we use the quantity

$$\mathrm{d}_i^k(E) = \frac{\sigma_i^K(E) - \sigma_i^{K-1}(E)}{(2K-1)\sigma_i^{K-1}(E)} \tag{26}$$

that gives the relative difference of these state-selected cross-sections for K and $K - 1$, weighted by the difference of the squares of the azimuthal quantum numbers. In Figure 3, this relative difference is plotted for the reactants in their vibrational ground states. The difference is large for low translational energies and decreases with both energy and quantum number K. Particularly large differences can be observed between $K = 0$ and $K = 1$ (more than 75% deviation between $E_{trans} = 400$ and 1000 cm^{-1}). For $E_{trans} > 1400$ cm^{-1}, the differences rapidly converge to a K-independent value which rises slowly with energy. At high translational energie (see Figure 3b), this value is on the order of 0.2−0.1%. A similar situation is found for initial excitation of the umbrella bending mode with one quantum (Figure 4). Here, however, the deviations are much smaller (at most up to 10% with fast convergence down to values below 1% for $E_{trans} > 1000$ cm^{-1}). Note that these values are very similar to those found for the ground state. Analogous observations can be made for other initial states and higher values of K, indicating a universal behavior especially for larger K and higher translational energies.

The difference between the cross-sections summed over all K values from the rotating-top approximation and from K-shifting are shown in Figure 5. In the latter model, the cross-section from ref 45, $\sigma^{K=0}$, is shifted by E^K_{trans}, omitting the contributions from $J < K$, and the resulting curves are summed up. While the results are very similar qualitatively, in particular for vibrational state (0, 0, 0), the differences are on the order of a factor of 2 [for (0, 1, 1)] or even larger [for (1, 0, 0)]. Consistent with Figure 4, the K-shifting cross-sections are larger (they would yield a relative difference of zero instead of a negative value), and the difference rises with energy, i.e., the available values for K. We note that the pronounced structure of the K-shifting cross-sections is due to interpolation effects.

B. Rate Constants. The rate constants calculated according to the theory presented above are shown in Figure 6 for the temperature range $10 < T < 1000$ K, together will two enlargements (from 50 and 285 K, respectively, to 1000 K). In addition to our reduced-dimensionality quantum treatment, we also present results obtained with the J and K shifting models, with all CH_3Cl rotations excluded and from transition state theory (TST) with two different potential surfaces. Except for

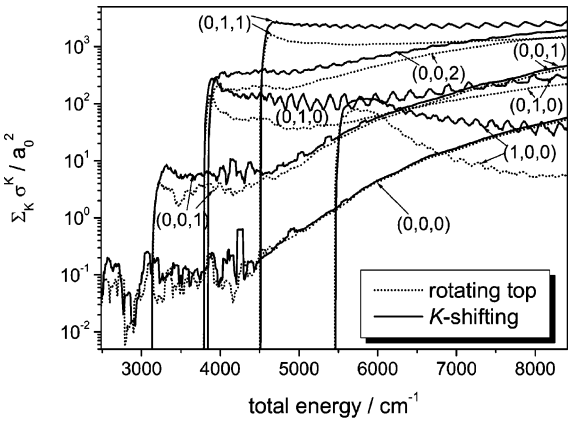

Figure 5. Comparison of cumulative state-selected cross-sections, summed over all final states and all energetically accessible states with azimuthal rotation labeled by *K*. The dotted curves represent the data obtained by the rotating-top approximation [cf. eq 11], while the solid ones are computed from the cross-section for $K = 0$ by adding this curve to itself for every *K* with the appropriate energy shift, omitting the contributions from $J < K$. The oscillations are due to interpolation effects. All curves are averaged over 80 cm^{-1}.

the RD quantum curve, the results in Figure 6a have already been presented in ref 45. Note that the "red. dim. quantum" curve from this reference is labeled here by "*K*-shifting, lower resolution". Despite the extreme computational effort of the calculations (see section II. E), we now have further increased the energetic resolution down to 10^{-1} cm^{-1}. All curves show a linear Arrhenius behavior in both the high- and low-temperature regimes with a slope greater in magnitude in the first limit, which is characteristic for a reaction with tunneling through a single barrier.[63]

In Figure 6b, the influence of *J*-shifting and *K*-shifting is shown. While increasing the resolution has quite a strong effect on the rate constant below room temperature, inclusion of *K* via the RTA has only a small effect, yielding a very slight decrease of the rate constant, i.e., farther away from the experimental value. Thus, the azimuthal rotation is of minor influence in this system, in accordance with the expectation from the overall small decrease of the cross-sections in the RTA model (cf. Figure 5). *J*-shifting, on the contrary, leads to significantly lower rate constants in all temperature ranges. These findings strongly support our conclusions drawn in ref 45 that (a) *J*-shifting is not appropriate for complex-forming reactions and (b) rotations (*j* rotations of the reactant and product symmetric tops) play a crucial role in the system. For chemically relevant temperatures starting from 250 K, the results from *K*-shifting and RTA are almost indistinguishable on the given scale, and resolution effects become negligible.

It remains to study the influence of the asymmetric modes (higher-frequency doubly degenerate C−H stretching and H−C−H bending modes) on the rate constants (see Figure 6c). We only present the combination with the RTA model and observe a slight increase of $k(T)$ where this effect becomes somewhat more pronounced for higher temperatures. The effect is significantly smaller than that going from *J*-shifting to RTA. Consequently, the asymmetric modes will have only a slight effect on the rate constants within this temperature range, as they are already expected to be largely overestimated in the asymmetric mapping model, and thus, their explicit inclusion cannot explain the discrepancy to the experimental value. Note that, in addition, the symmetric modes do not yield the dominant contribution to the rate constant (cf. Figure 7).

The influence of asymmetric modes compared to their symmetric counterparts has been studied explicitly by several

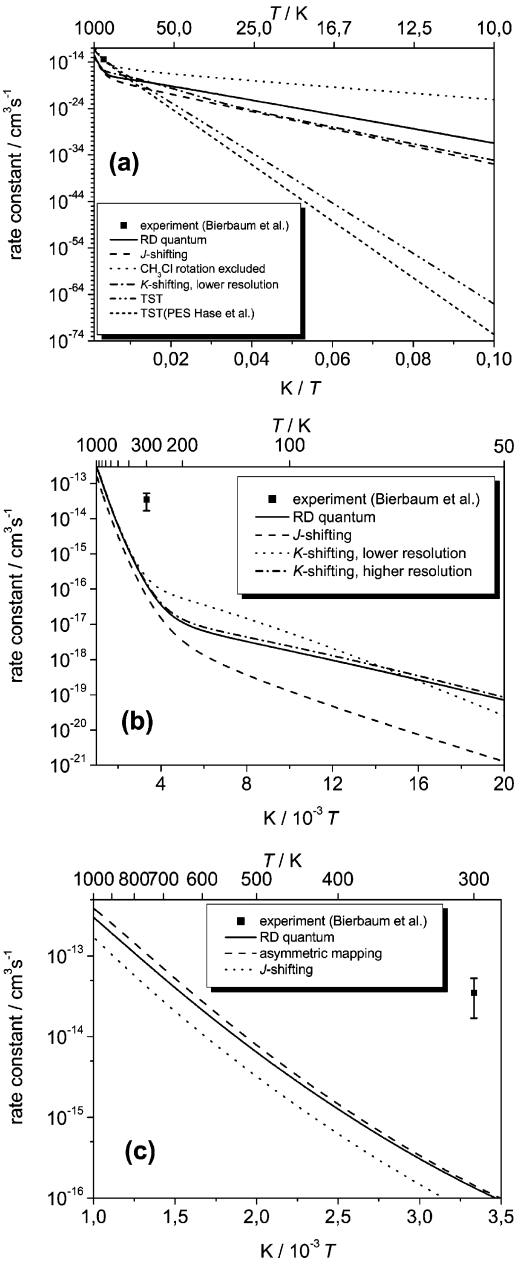

Figure 6. Thermal rate constant for the gas-phase S_N2 reaction $Cl^- + CH_3Cl' \rightarrow ClCH_3 + Cl'^-$. Eight different models are applied (for a description see the text).

others. Wang and Bowman found the symmetric stretch of the H_2O molecule in the $OH + H_2 \rightarrow H + H_2O$ reaction to be more populated than the corresponding antisymmetric mode,[64] whereas in the $H + C_2H_2 \rightarrow H_2 + C_2H$ reaction, the antisymmetric C−H stretch showed a higher effectivity to promote the reaction.[65] In the $O + CH_4 \rightarrow OH + CH_3$ reaction, which is the most comparable one to our investigations, calculations by Clary and Palma[66] resulted in a smaller reaction probability for the antisymmetric C−H stretch, but of comparable magnitude. Experiments on the $Cl + CH_4 \rightarrow HCl + CH_3$ reaction[67] show almost indistinguishable state-selected differential cross-sections and rovibrational distributions when the reactants are excited either in the symmetric or antisymmetric C−H streching vibration. However, in all of these reactions, the antisymmetric mode is intrinsically coupled to the reaction coordinate, which is not the case for our reaction.

In Figure 7, the contributions of the various initial vibrational states to the total rate constant are analyzed in detail. The various

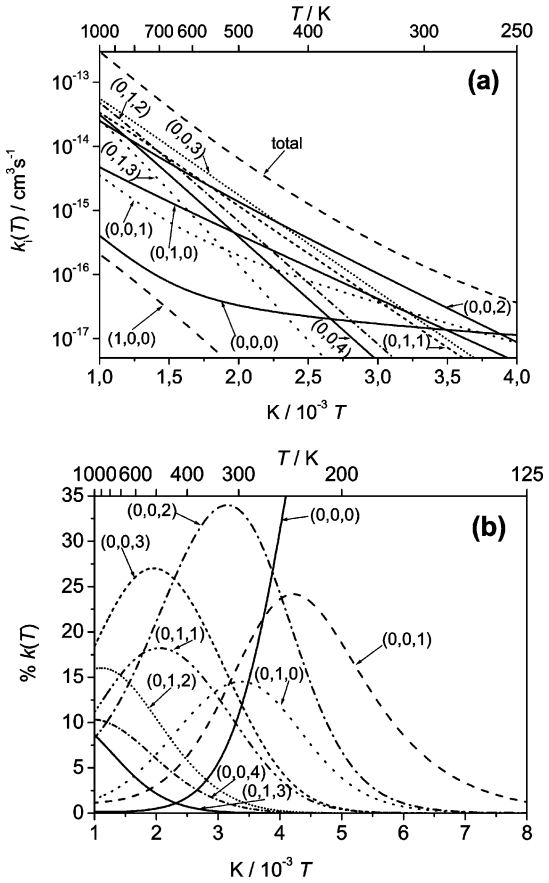

Figure 7. Contribution of the individual reactant vibrational states to the thermal rate constant in the reduced-dimensionality quantum model, i.e., summed over all J and K. (a) Absolute state-selected rate constants. (b) Percentage contribution of the reactant vibrational states.

curves show a linear Arrhenius behavior within the selected temperature range and a lot of crossings; the ground state itself shows two different slopes, as does the total rate constant (with a different bridging region, however), cf. ref 63. This is very different compared to non-complex-forming bimolecular reactions. A comparable system (however with light atoms only), the abstraction reaction between a hydrogen atom and methane/methanol, was recently studied by Kerkeni and Clary with a state-selective analysis of the rate constants.[68,69] A direct comparison of the overall behavior is difficult, because the higher barriers in these reactions cause the relevant interesting features to appear at higher, rarely investigated temperatures, and the smaller number of degrees of freedom considered yields less curves.

The relative contributions of the different initially excited vibrational states are shown in Figure 7b. The individual curves show a strikingly similar shape. Under thermal conditions, the state with two quanta in the C−Cl stretching mode (0, 0, 2) of the reactant molecule contributes most (35%), followed by the umbrella bend (0, 1, 0) and one or three quanta in the C−Cl stretch (0, 0, 1)/(0, 0, 3) (15% each). The combination mode (0, 1, 1) and the vibrational ground state (0, 0, 0) contribute with 10% each. In general, excitations with quanta in the umbrella mode contribute less than pure excitations of the C−Cl bond, which is one of the reasons for the low influence of the asymmetric modes (cf. Figure 6c). Note that the (0, 0, 2) mode opens at a total energy of 1432 cm^{-1} above the ground state of CH_3Cl, which is about seven times as large as the average thermal energy at room temperature. Similar observations hold for other temperatures, which infers that fairly high energies

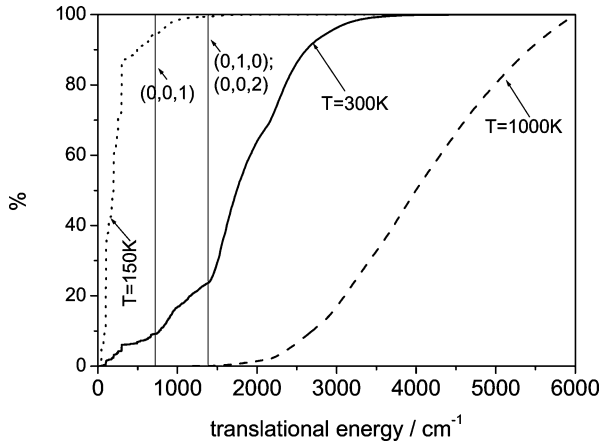

Figure 8. Contribution of different translational energies to the rate constants at $T = 150$ K, $T = 300$ K, and $T = 1000$ K. For each temperature, the graph shows the ratio $k_E(T)/k_{E_{max}}(T)$, where $k_E(T)$ is obtained by cutting the integral in eq 20 at translational energy E and E_{max} is the highest translational energy for which cross-sections have been computed. Opening of the first three stretching modes (0, 0, 1), (0, 1, 0) and (0, 0, 2) is indicated by the vertical lines.

are relevant for this reaction as the corresponding modes are much more effective in promoting the reaction than the low-lying ones.

To shed more light on the contribution of different translational energies on the rate constants, we evaluate the ratio $k_E(T)/k_{E_{max}}(T)$ by computing the integral in eq 20 at translational energy E. The quantity E_{max} denotes the highest energy for which cross-sections have been computed in the present work. Results are shown in Figure 8 for three different temperatures (150, 300, and 1000 K). For each temperature, the major contribution to the rate constant stems from an energetic region far above the average thermal energy. At room temperature, about 80% can be traced back to the translational energy above 1400 cm^{-1} where the (0, 1, 0) and (0, 0, 2) modes open up, which is consistent with Figure 7. For $T = 1000$ K, we conclude that the value for the rate constant is not fully converged, as the slope of the displayed curve does not approach zero for $E_{max} = 6000$ cm^{-1} which is still nine times as large as the average thermal energy at this temperature. The negative curvature above $E = 5000$ cm^{-1} implies convergence on the order of magnitude, however, which justifies the inclusion of these high temperatures in our plots.

In Figure 9, the cumulative contributions c of angular momenta to the rate constant are given as a function of $1/T$. The unusual scaling of the ordinate results from plotting $100\% - c$ on a logarithmic scale in order to demonstrate the deviation of the RTA/RLA model (c,d) from J-shifting (a,b); in the latter model, the resulting curves are straight lines as inferred by the rotational partition function. For each model, two different temperature regimes are shown. The ordinates are labeled by the values of c itself. If curves are not labeled, the maximum value of J increases by 10 for each curve from the first to the last corresponding label. For temperatures starting at $T = 10$ K, we observe a very irregular pattern and several jumps with respect to the individual contributions of the total angular momenta. These features cannot be attributed to a physical origin, but are consequences of the limited energy grid size: The individual probabilities $P^J(E)$ do not have a fully resolved resonance structure, resulting in under/overweighing of the individual contributions. However, summation of these yields results that are also reliable for low temperatures in the order of magnitude: Even for the most striking irregularity at $T =$

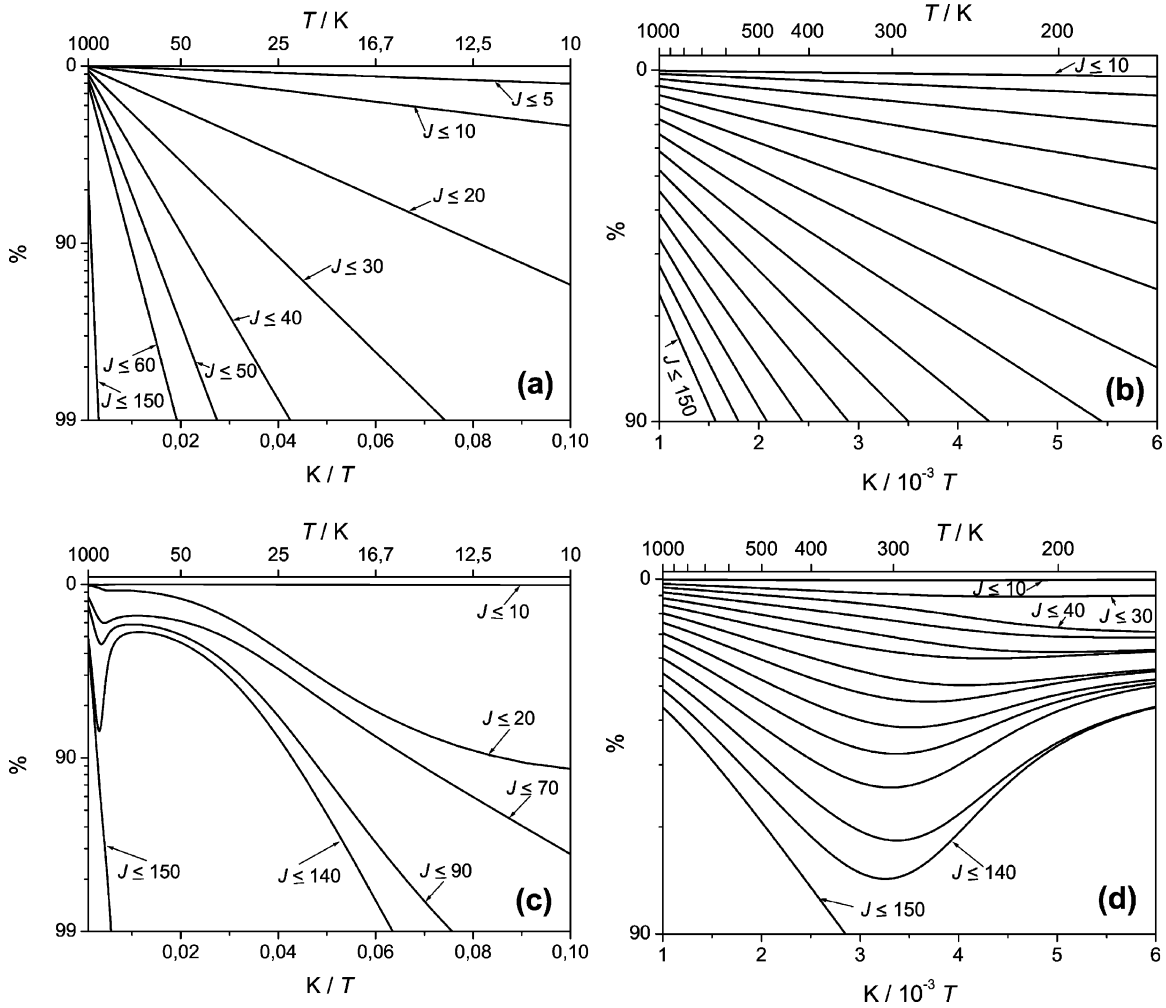

Figure 9. Cumulative contribution c of angular momenta to the rate constant as a function of $1/T$ (see the text).

50 K where the large gap between $J = 140$ and $J = 150$ is clearly due to the energy resolution, the contribution of $J \leq 140$ is still 50%. The increasing importance of higher angular momenta shows a clear deviation from the linear behavior in the J-shifting, which for values from $T = 100$ K up to room temperature is due to the dominant contributions of energetically higher modes; the smaller amount of kinetic energy left in these modes favors smaller angular momenta. From a starting point at $T = 250$ K, the distances of the curves become increasingly regular, indicating less importance of the energy resolution in this temperature region, consistent with Figure 6. Above $T = 400$ K, the curves become straight lines as in the J-shifting model with the only difference that more angular momenta contribute to the final value. This observation, which is also valid for the low-temperature regime, explains the overall lower rate constants obtained by J-shifting.

IV. Conclusions

(1) On the basis of Bowman's adiabatic rotation approximation in quantum reactive scattering, the rotating-top approximation is introduced that allows for explicit consideration of the rotational quantum number K in reduced-dimensionality calculations for reactions with true symmetric-top geometries during the entire collision process.

(2) Time-independent quantum scattering calculations have been carried out for the S_N2 reaction $Cl^- + CH_3Cl' \rightarrow ClCH_3 + Cl'^-$ using hyperspherical coordinates describing the bonds being broken and formed. The two totally symmetric modes of the methyl group are included in the model, and C_{3v} symmetry is conserved throughout the reaction. By making use of the rotating-top approximation, converged state-to-state selected total reaction cross-sections, summed over all K-rotor contributions, could be calculated.

(3) The thermal rate constant has been calculated and compared with the ones obtained from more approximate models (J-shifting/K-shifting quantum and transition state theory). While TST rate constants show fortuitous good agreement with experiment, the physically more sound reduced-dimensionality quantum calculations show large deviations from the only available experimental data point.

(4) Contributions of the individual K quantum numbers in the rotating-top approximation have been analyzed and found to decrease the cross-sections in an overall small amount compared to K-shifting. The resulting differences of the rate constants are negligible with respect to the order of magnitude.

(5) A new model has been proposed to estimate the influence of asymmetric modes when quantum results for the symmetric counterpart are available, indicating a negligible influence on the rate constant at room temperature.

(6) State-selected and energy-dependent rate constants have been analyzed. The results underline the importance of certain energetically high modes even at low temperatures, especially those with excitations in the C−Cl-bond.

(7) An analysis of the contribution of the different total angular momenta showed the convergence for small tempera-

tures to occur only via summation. The lower rate constants of *J*-shifting could be traced back to contributions of higher angular momenta.

Acknowledgment. This work was supported by the Deutsche Forschungsgemeinschaft through grant SCHM 1651/1-1. Additional support from the Fonds der Chemischen Industrie is gratefully acknowledged.

References and Notes

(1) Bowman, J. M. *Adv. Chem. Phys.* **1985**, *65*, 61.
(2) Bowman, J. M.; Wagner, A. F. In *The Theory of Chemical Reaction Dynamics*; Clary, D. C., Ed.; Reidel: Dordrecht, 1986; p 47.
(3) Walker, R. B.; Hayes, E. F. In *The Theory of Chemical Reaction Dynamics*; Clary, D. C., Ed.; Reidel: Dordrecht, 1986; p 105.
(4) Bowman, J. M. *J. Phys. Chem.* **1991**, *95*, 4960.
(5) Bowman, J. M.; Wang, D. In *Advances in Molecular Vibration and Collision Dynamics*; Bowman, J. M., Ed.; JAI: Greenwich, CT, 1994; Vol. II B, p 187.
(6) Dzegilenko, F. N.; Bowman, J. M. *J. Chem. Phys.* **1996**, *105*, 2280.
(7) Child, M. S. *Mol. Phys.* **1967**, *12*, 401.
(8) Bowman, J. M. *Chem. Phys. Lett.* **1994**, *217*, 36.
(9) Bowman, J. M. *J. Phys. Chem. A* **1998**, *102*, 3006.
(10) Bowman, J. M. *Theor. Chem. Acc.* **2002**, *108*, 125.
(11) Hase, W. L. *Science* **1994**, *266*, 998.
(12) Chabinyc, M. L.; Craig, S. L.; Regan, C. K.; Brauman, J. I. *Science* **1998**, *279*, 1882.
(13) Laerdahl, J. K.; Uggerud, E. *Int. J. Mass Spectrom. Ion Processes* **2002**, *214*, 277.
(14) Schmatz, S. *ChemPhysChem* **2004**, *5*, 600.
(15) Olmstaed, W. N.; Brauman, J. I. *J. Am. Chem. Soc.* **1977**, *99*, 4219.
(16) Dodd, J. A.; Brauman, J. I. *J. Phys. Chem.* **1986**, *90*, 3559.
(17) Barlow, S. E.; VanDoren, J. M.; Bierbaum, V. M. *J. Am. Chem. Soc.* **1988**, *110*, 7240.
(18) Tucker, S. C.; Truhlar, D. G. *Chem. Phys. Lett.* **1989**, *157*, 164.
(19) Vande Linde, S. R.; Hase, W. L. *J. Phys. Chem.* **1990**, *94*, 2778.
(20) Vande Linde, S. R.; Hase, W. L. *J. Chem. Phys.* **1990**, *93*, 7962.
(21) Cho, Y. J.; Vande Linde, S. R.; Zhu, L.; Hase, W. L. *J. Chem. Phys.* **1992**, *96*, 8275.
(22) Hase, W. L.; Cho, Y. J. *J. Chem. Phys.* **1993**, *98*, 8626.
(23) Brauman, J. I. *J. Mass Spectrom.* **1995**, *30*, 1649.
(24) DeTuri, V. F.; Hintz, P. A.; Ervin, K. M. *J. Phys. Chem.* **1997**, *101*, 5969.
(25) Clary, D. C.; Palma, J. *J. Chem. Phys.* **1997**, *106*, 575.
(26) Mann, D. J.; Hase, W. L. *J. Phys. Chem. A* **1998**, *102*, 6208.
(27) Su, T.; Hase, W. L. *J. Phys. Chem. A* **1998**, *102*, 9819.
(28) Schmatz, S.; Clary, D. C. *J. Chem. Phys.* **1998**, *109*, 8200.
(29) Li, G.; Hase, W. L. *J. Am. Chem. Soc.* **1999**, *121*, 7124.
(30) Ervin, K. M. *Int. J. Mass Spectrom.* **1999**, *187*, 343.
(31) Hernández, M. I.; Campos-Martinez, J.; Villarreal, P.; Schmatz, S.; Clary, D. C. *Phys. Chem. Chem. Phys.* **1999**, *1*, 1197.
(32) Schmatz, S.; Clary, D. C. *J. Chem. Phys.* **1999**, *110*, 9483.
(33) Yu, H. G.; Nyman, G. *Chem. Phys. Lett.* **1999**, *312*, 585.
(34) Schmatz, S. *Chem. Phys. Lett.* **2000**, *330*, 188.
(35) Kato, S.; Davico, G. E.; Lee, H. S.; Depuy, C. H.; Bierbaum, V. M. *Int. J. Mass Spectrom.* **2001**, *210*/*211*, 223.
(36) Angel, L. A.; Ervin, K. M. *J. Phys. Chem. A* **2001**, *105*, 4042.
(37) Sun, L.; Hase, W. L.; Song, K. *J. Am. Chem. Soc.* **2001**, *123*, 5753.
(38) Schmatz, S.; Botschwina, P.; Hauschildt, J.; Schinke, R. *J. Chem. Phys.* **2001**, *114*, 5233.
(39) Hauschildt, J.; Schinke, R.; Schmatz, S.; Botschwina, P. *Phys. Chem. Chem. Phys.* **2001**, *3*, 2275.
(40) Angel, L. A.; Garcia, S. P.; Ervin, K. M. *J. Am. Chem. Soc.* **2002**, *124*, 336.
(41) Schmatz, S.; Botschwina, P.; Hauschildt, J.; Schinke, R. *J. Chem. Phys.* **2002**, *117*, 9710.
(42) Angel, L. A.; Ervin, K. M. *J. Am. Chem. Soc.* **2003**, *125*, 1014.
(43) Schmatz, S.; Hauschildt, J. *J. Chem. Phys.* **2003**, *118*, 4499.
(44) Hennig, C.; Schmatz, S. *J. Chem. Phys.* **2004**, *121*, 220.
(45) Hennig, C.; Schmatz, S. *Phys. Chem. Chem. Phys.* **2005**, *7*, 1552.
(46) Schmatz, S. *J. Chem. Phys.* **2005**, *122*, no. 234206.
(47) Hennig, C.; Schmatz, S. *J. Chem. Phys.* **2005**, *122*, no. 234207.
(48) McCurdy, C. W.; Miller, W. H. In ACS Symposium Series 56; Brooks, P. R., Hayes, E. F., Eds.; American Chemical Society: Washington, DC, 1984; p 239.
(49) Bittererovà, M.; Bowman, J. M.; Peterson, K. *J. Chem. Phys.* **2000**, *113*, 6186.
(50) De Fazio, D.; Castillo, J. F. *Phys. Chem. Chem. Phys.* **1999**, *1*, 1165.
(51) Russel, C. L.; Manolopoulos, D. E. *J. Chem. Phys.* **1999**, *110*, 177.
(52) Pack, R. T. *J. Chem. Phys.* **1974**, *60*, 633.
(53) McGuire, P.; Kouri, D. J. *J. Chem. Phys.* **1974**, *60*, 2488.
(54) Schatz, G. C. *Chem. Phys. Lett.* **1988**, *150*, 92.
(55) Clary, D. C. *J. Chem. Phys.* **1991**, *95*, 7298.
(56) Echave, J.; Clary, D. C. *J. Chem. Phys.* **1994**, *100*, 402.
(57) Pogrebnya, S. K.; Echave, J.; Clary, D. C. *J. Chem. Phys.* **1997**, *107*, 8975.
(58) Kuppermann, A.; Kaye, J. A.; Dwyer, J. P. *Chem. Phys. Lett.* **1980**, *74*, 257.
(59) Römelt, J. *Chem. Phys. Lett.* **1980**, *74*, 263.
(60) Colbert, D. T.; Miller, W. H. *J. Chem. Phys.* **1992**, *96*, 1982.
(61) Echave, J.; Clary, D. C. *Chem. Phys. Lett.* **1992**, *190*, 225.
(62) Stechel, E. B.; Walker, R. B.; Light, J. C. *J. Chem. Phys.* **1978**, *69*, 3518.
(63) Bell, R. P. *Proc. R. Soc. London, Ser. A* **1933**, *139*, 466.
(64) Wang, D.; Bowman, J. M. *J. Chem. Phys.* **1992**, *96*, 8906.
(65) Wang, D.; Bowman, J. M. *J. Chem. Phys.* **1994**, *101*, 8646.
(66) Palma, J.; Clary, D. C. *Phys. Chem. Chem. Phys.* **2000**, *2*, 4105.
(67) Bechtel, H. A.; Camden, J. P.; Ankeny Brown, D. J.; Zare, R. N. *J. Chem. Phys.* **2004**, *120*, 5096.
(68) Kerkeni, B.; Clary, D. C. *J. Chem. Phys.* **2004**, *120*, 2308.
(69) Kerkeni, B.; Clary, D. C. *J. Chem. Phys.* **2004**, *121*, 6809.